ELSEVIER

Journal of Alloys and Compounds 311 (2000) 256–264

Journal of ALLOYS AND COMPOUNDS

www.elsevier.com/locate/jallcom

Crystal structure and morphology of a new compound, LiB

Zhijian Liu*, Xuanhui Qu, Baiyun Huang, Zhiyou Li

State Key Laboratory for Powder Metallurgy, Central-South University of Technology, Changsha, Hunan 410083, PR China

Received 31 December 1999; accepted 31 May 2000

Abstract

The crystal structure and morphology of the compound LiB, used as a refractory frame in the advanced thermal battery anode of Li–B alloys, have been determined. The X-ray diffraction (XRD) pattern of the compound indicates that its composition is LiB, it belongs to space group No.194, $P6_3/mmc$, with hexagonal structure, $a = 0.4022$ nm and $c = 0.2796$ nm. In the unit cell, B atoms occupy the position (2*b*) (0,0,1/4) and Li (2*c*) (1/3,2/3,1/4). The theoretical density of the compound is 1.50 g/cm^3. SEM results indicate that the compound is in the form of a fiber with random orientation. After rolling, the LiB fibers align along the rolling direction. The corresponding texture has been verified by X-ray photography and XRD patterns, and it fits well with theoretical predictions. © 2000 Elsevier Science S.A. All rights reserved.

Keywords: LiB compound; Li–B alloy; Crystal structure

1. Introduction

Lithium and boron are metallic and non-metallic elements, respectively, with a small atomic number. Study of their compounds is beneficial both in theory and for potential applications. A new lithium–boron compound with a composition ratio near 1:1 [1–4] has attracted much attention because of its important role in a recently developed anode material of a thermal battery. The preparation technology of Li–B alloys (Li–30 wt% B) was first reported by Wang [5]. In his report, a new refractory, high strength and porous Li–B compound was produced after two exothermic reactions (~330 and ~530°C). The remaining lithium metal soaks into the pores of the Li–B compound frame.

The electrochemical properties of the Li–B alloy are nearly the same as that of pure lithium. However, its melting point is close to 1000°C, which is much higher than that of pure lithium (180.6°C), implying that the Li–B alloy is, following Li–Al and Li–Si thermal battery anode materials [6], the best for its high energy and power density.

There are several reports on the chemical composition and crystal structure of the Li–B compound. From a differential thermal analysis (DTA) experiment, Wang [7] proposed that its chemical composition is Li_5B_4. With further XRD, neutron diffraction and nuclear magnetic resonance (NMR) analyses, Wang and Mitchell [1] further proposed that the crystal structure of Li_5B_4 is rhombohedral (*R3m*) with $a = 0.493$ nm and $\alpha = 90°$ and the structure is disordered in such a way that its long range symmetry is body-centered cubic (*I43m*) with $a = 0.493$ nm. However, there are still many problems with the rhombohedral structure model. Many reflections of the XRD pattern of the compound do not yet fit. Further, a subtle differential scanning calorimetry (DSC) analysis by Dalleck and Ernst [2] showed that the chemical composition is Li_7B_6, which is also verified by other researchers [8] and widely accepted. $Li_{1.06}B$ [9] and LiB [3] have also been proposed for this compound. It is clear that the ratio of Li to B in the compound is approximately one, but its crystal structure and morphology are still unclear. The uncertainty in the basic knowledge of the crystal structure and morphology of the compound is one of the reasons why the advanced thermal battery anode Li–B alloy is still not beyond the laboratory stage. It also impedes further study of this new compound. The goal of the work presented in this paper was to obtain more accurate crystal structure information about the Li–B compound.

*Corresponding author.
E-mail address: lzpm@mail.csut.edu.cn (Z.J. Liu).

0925-8388/00/$ – see front matter © 2000 Elsevier Science S.A. All rights reserved.
PII: S0925-8388(00)01076-8

2. Experimental

Two different samples were prepared. Sample 1 was synthesized in an iron crucible with 0.6 g of lithium (purity >99.9 wt%) and 0.4 g of crystalline boron (purity >99 wt%, −80 mesh). The synthesis process, consisting of two exothermic reactions (~330 and ~530°C), was accomplished in argon. The sample was used directly for XRD analysis without any mechanical deformation. Sample 2 was obtained using the stirring technique [7] with 70 g of Li and 34 g of amorphous boron powder (purity >90 wt%, with O and Mg as impurities). The temperature was carefully controlled to prevent the second reaction from ignition by the first exothermic reaction [7]. It was rolled into a 0.32 mm thick film to investigate its deformation behavior.

Furthermore, in order to observe the morphology of the Li–B compound, the samples were placed in tetrahydrofuran (THF)–naphthalene solution [10] for 1 week to extract free lithium.

The XRD experiment was carried out on a BD86 diffractometer with Cu Kα radiation and a graphite single crystal monochromator. The specimen support frame was covered by plastic film to protect the specimen from reaction with humid air.

For the Laue photograph in transmission mode, Cu Kα and a Ni filter were used.

An S-650 SEM was used to observe the microstructure. The exposure time of the samples to air was <1 s.

All operations on both Li and Li–B alloys were completed in a glove box with a relative humidity of $R_H \leq 2\%$.

3. Results

3.1. XRD patterns

Fig. 1 shows the XRD pattern of sample 1. It shows some reflections of Li [11], Li_2O [12] and Li_3B_{14} [13] in the low diffraction angle zone. The remaining reflections are caused by the Li–B compound.

Fig. 2a,b shows the XRD patterns of sample 2 before and after rolling. After rolling, some diffraction reflections disappear ($2\theta = 41.3°$, 62.77°, etc.), which shows the existence of texture in the Li–B compound.

3.2. X-ray Laue photograph

Fig. 3 shows the X-ray transmission Laue photograph of sample 2. Besides the Li–B compound diffraction circle, there are also circles of Li, Li_2O and the plastic film. The intensity of the Li–B compound on the circles is not uniform, indicating the textural character of sample 2.

3.3. SEM photograph

Fig. 4a,b shows SEM photographs of sample 1, indicating the random fibrous structure of the Li–B compound. Fig. 4c,d shows SEM photographs of sample 2. It is found that, after rolling, the fibers of the Li–B compound align along the rolling direction.

4. Discussion

4.1. Determination of diffraction indices of XRD data of the Li–B compound

Because of the low atomic numbers of the elements Li and B, the Li–B alloy sample is readily amenable to X-rays. If the sample is thick, the reflection will shift to a low angle and broaden unsymmetrically [14]. The side-by-side diffraction reflections can therefore be separated for a thin sample only. However, a decrease in thickness will reduce the diffraction intensity. Therefore, a long time is needed to obtain a sufficient diffraction intensity, which will result in more oxidation of the sample surface. This is the reason why the lithium oxide reflections are present in the low diffraction angle zone (Fig. 2a). In addition, the reflections of lithium and Li_3B_{14} are also present in the low diffraction angle zone. They do not interfere with the reflections of the Li–B compound. The remaining reflections include the reflections from Li_5B_4 [7], Li_7B_6 [2] and $Li_{1.06}B$ [9]. It is found using a graphical method [14] that the compound belongs to the hexagonal crystal system. Otherwise, if the cubic model proposed by Wang and Mitchell [1] is used, many experimental reflections ($2\theta =$ 41.3°, 62.77°, 80.59°, etc.) have to be excluded and many theoretical reflections of the cubic model do not agree with the experimental ones, which were assumed to come from an unknown new phase. Those reflections have now been well indexed with the hexagonal model.

From the high angle ($2\theta = 150°$) diffraction reflection data the lattice constants are calculated to be $a = 0.4022$ nm and $c = 0.2796$ nm. Table 1 gives a comparison of XRD data from different authors.

4.2. Unit cell model and calculation of diffraction intensity

4.2.1. Calculation method

In general, Rietveld refinement is the best way to analyze an XRD pattern. For the XRD patterns in this paper, the precision of the reflections was affected by reflections from Li, Li_2O and Li_3B_{14}. In addition, the strong penetration of X-rays into the Li–B alloy sample also greatly affects the relative intensity and positions of the reflections of the Li–B compound. Therefore, only a relative integrated intensity computation was carried out.

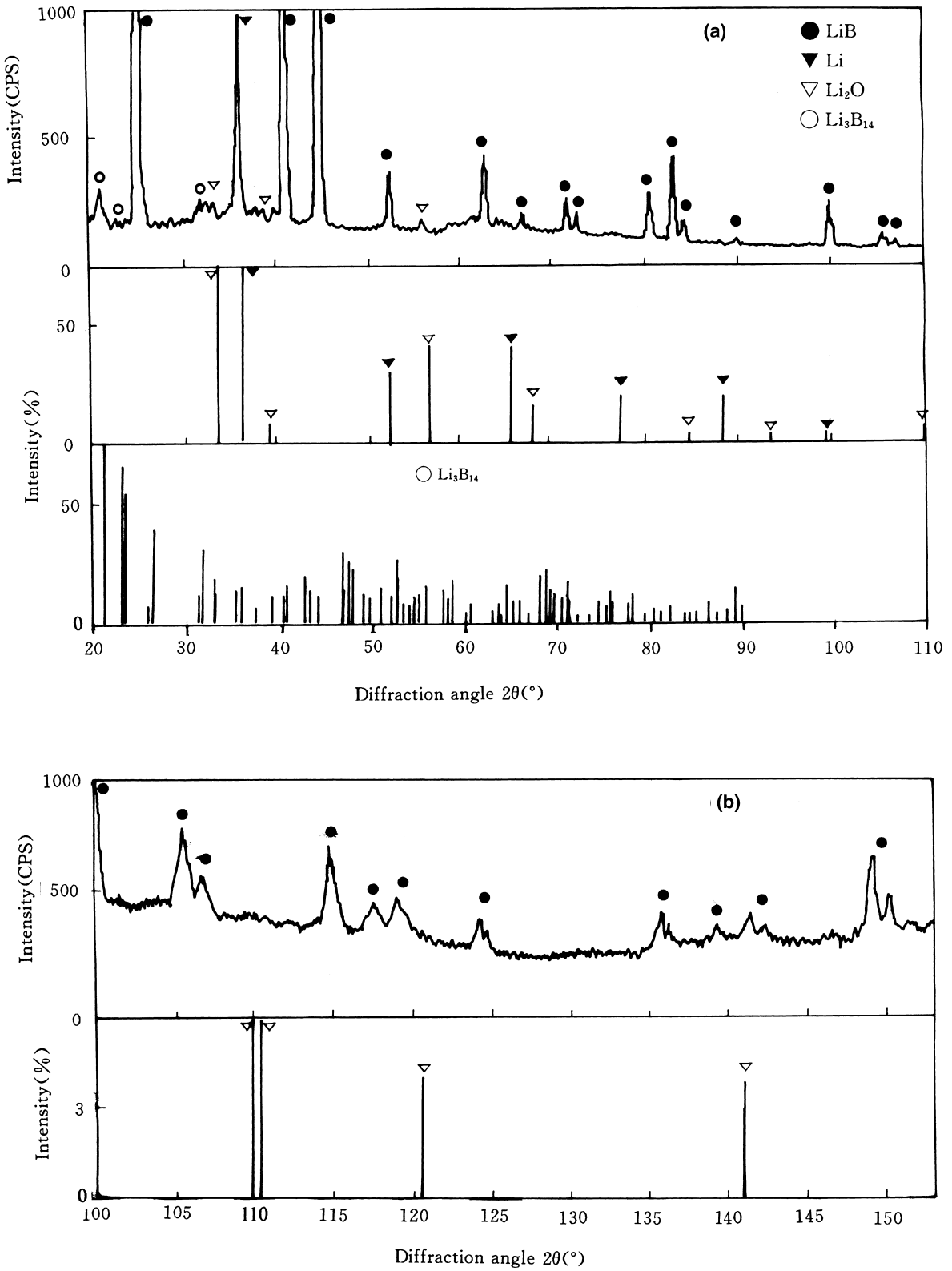

Fig. 1. XRD pattern for sample 1. Test conditions: (a) slit system, 1° −0.32–1°; current, 24 mA; voltage, 40 kV; scanning rate, 0.5°/min. (b) Slit system, 4° −0.6–4°; current, 24 mA; voltage, 40 kV; scanning rate, 0.5°/min.

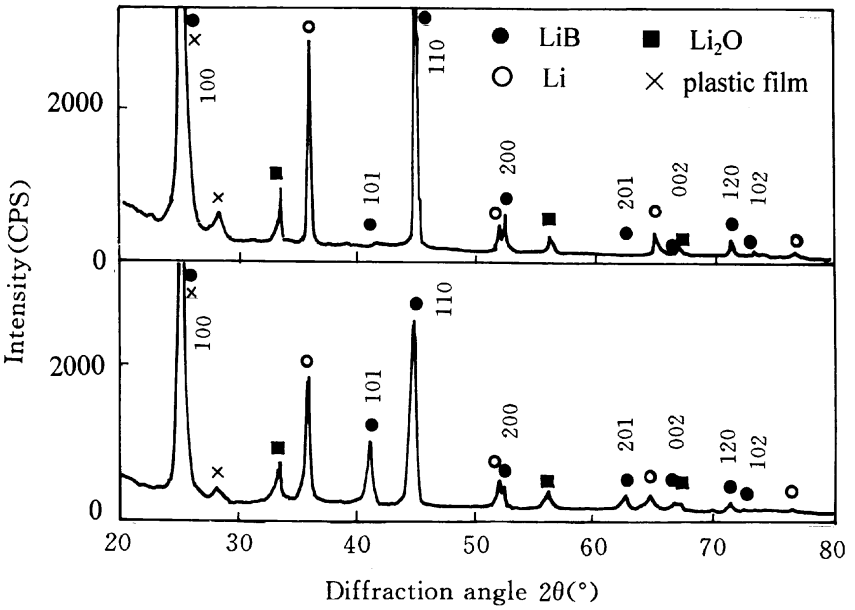

Fig. 2. XRD patterns for sample 2: (a) before rolling; (b) after rolling.

In the calculation of the relative integrated intensity, some corrections are taken into account. Because the value of the absorption parameter, μ, is small for both Li and B, intensity loss caused by transmission has been considered.

In this mode, diffraction intensity data were obtained from the measured reflection heights. Since the diffraction intensity is affected by the reflection width, the data should be corrected. In our work, the reflection width of the apparatus was derived from an experiment with a high-purity Si powder sample.

4.2.2. Unit cell of the LiB compound and relative diffraction intensity

The unit cell was determined as shown in Fig. 5. Based on the structure, the structure factor F^2_{hkl} can be calculated. The result of the calculation shows that there are only three possible cases for all reflections. First, for the 101, 201 and 121 reflections, F^2_{hkl} only depends on the atomic scattering factor of lithium, $F^2_{hkl} = 3f^2_{Li}$. Second, for the 100, 200, 210, 102, 202, 130 and 122 reflections, boron is dominant, $F^2_{hkl} = (2f_B - f_{Li})^2$. Finally, for the 110, 300, 112, 220, 002,

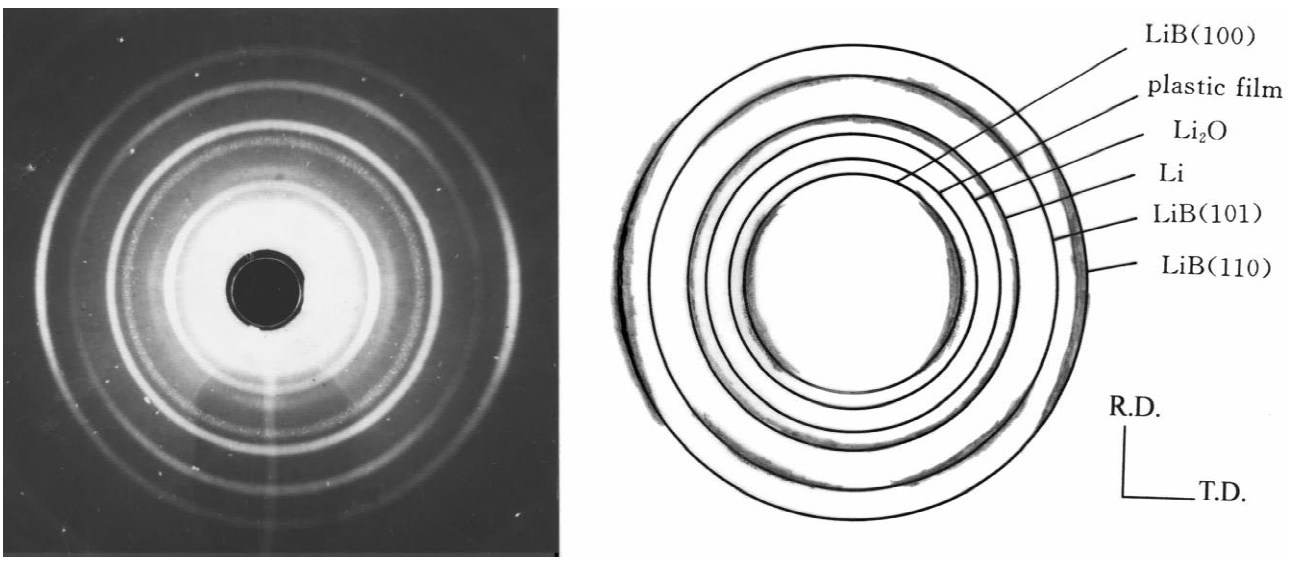

Fig. 3. Laue photograph of XRD for sample 2. Test conditions: target, Cu Kα; filter, Ni film; current, 20 mA; voltage, 35 kV; time, 6 h, $l_0 = 29.4$ mm.

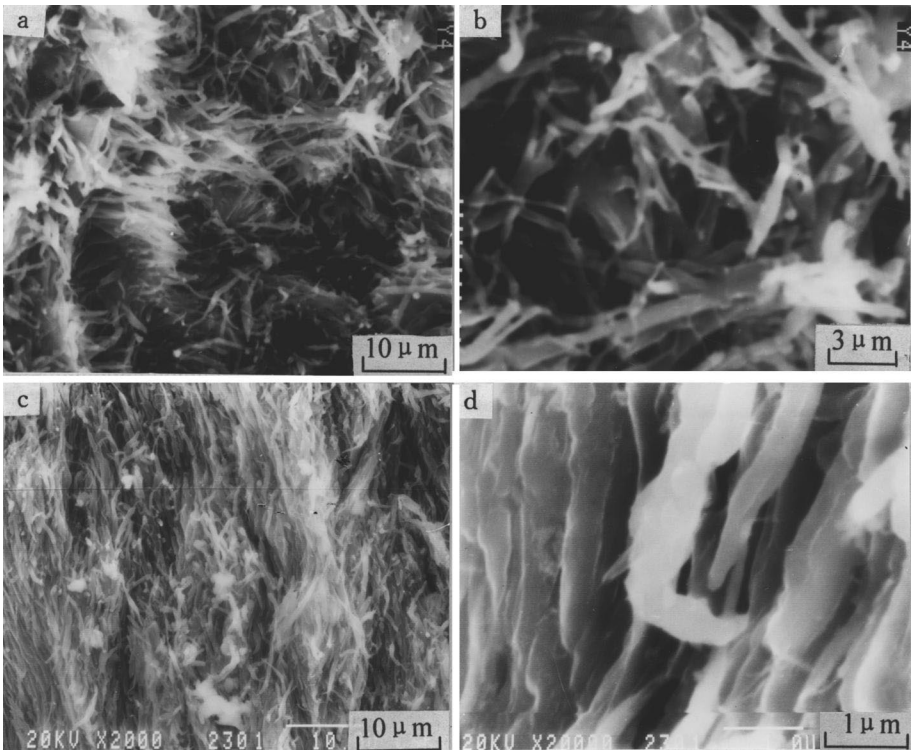

Fig. 4. SEM photographs of the LiB compound. (a,b) Sample 1 without rolling; (c,d) sample 2 rolled.

101, 201 and 121 reflections, both lithium and boron play the same role, $F_{hkl}^2 = 4(f_{Li} + f_B)^2$. Comparing the calculated results with experimental data, $\bar{u}_{Li\sigma}$, $\bar{u}_{Lic}$, $\bar{u}_{B\sigma}$, $\bar{u}_{Bc}$ can be determined.

Table 2 compares the calculated results with observed results. As can be seen, almost all the positions of the observed reflections are lower than those calculated. The zero point correction is based on the calculation of high angle reflection ($2\theta = 150°$). The shifts observed come from the penetration of X-rays into the sample. The lower the diffraction angle (2θ), the more the shift [14]. For the best fitted result, I_1, the value of $\bar{u}_{Bc}$ is very large, but the intensity error of reflection 112 is unacceptable. The errors of further reflections $hk2$ (I_2) increase as $\bar{u}_{Bc}$ decreases.

In the calculated result, the value of the thermal displacement parameter $\bar{u}_{Bc}$ is very large. Although the original meaning of $\bar{u}_{Bc}$ is the mean amplitude of the thermal vibration [15], it reflects practically the distribution character of scattering electrons along the ⟨001⟩ direction around the boron atom. If taken as the result of the thermal vibration of B atoms, it would be unreasonable that $\bar{u}_{Bc}$is greater than $\bar{u}_{Lic,}$ because the Li atom is lighter than the B atom. With decreasing temperature, the corresponding weak reflection intensities should increase. In practice, this kind of phenomenon was not discovered in Wang's work [7]. There may be another reason leading to this unusual result.

In general, B atoms in borides can easily form covalent bonds. With increasing B content in borides, covalent couples, chains and nets between B atoms readily form [16]. In the compound LiB, boron covalent chains exist along the *c*-axis. These should lead to a high density of electrons between the B atoms along the *c*-axis. Because of the low atomic numbers of Li and B, scattering electrons are rare around these atoms. The scattering contribution from covalent electrons cannot be neglected. This might be one of the reasons that led to a larger error for the 112 reflection intensity in our calculation.

From nuclear magnetic resonance experiments, Sanchez and Belin [9] found that the Li in the LiB compound is Li^+. Mitchell and Sutula [17] discovered that the compound LiB is an electrical conductor. Therefore, covalent and ionic bonds may co-exist in the compound. According to the crystal structure and physical character, the compound LiB is considered to be a polyanionic compound, a Zintl compound [18]. For the Zintl phase, the octet rule can be applied:

$$b(xx) = 8 - N \quad (1)$$

where $b(xx)$ is the number of covalent bonds of an anionic atom and N the valence electron number of an anionic atom.

Because one Li atom has transferred an electron to one B atom, after s–p hybridization every B atom has four valence electrons. Then $b(xx) = 4$, there are four covalent bonds for every B atom. To form equal lengths of covalent chains in the *c*-direction, the four valence electrons have to

Table 1
Comparison of XRD experimental results for the Li–B compound (Cu target)

No.	Sample 1			Wang [1]		Dalleck [2]		Sanchez [9]	
	2θ	I_0	*hkl*	2θ	I_0	2θ	I_0	2θ	I_0
1	25.47	100	100	25.40	100	25.70	100	25.52	100
2	41.30	23.5	101	[a]		40.80	23	41.25	11.2
3	44.98	57.8	110	44.87	65	45.10	65	44.95	56
4	52.44	3.6	200	52.44	11	52.60	<5	52.40	<2
5	62.77	4.1	201	[a]		62.25	<5	62.70	3.6
6	66.87	0.9	002						
7	71.59	1.9	120	71.53	5			71.50	<2
8	72.84	0.9	102						
9	80.59	2.8	121	[a]		79.90	<5		
10	83.09	5.0	300	83.01	13	82.75	<5		
11	84.22	1.2	112						
12	89.95	0.3	202						
13	100.05	3.2	220	99.81	9	99.55	<5		
14	105.82	1	130						
15	106.99	0.4	122						
16	114.98(a_1)		131						
	115.32(a_2)								
17	117.78		103						
18	119.23(a_1)		302						
	119.66(a_2)								
19	124.39(a_1)		400						
	124.81(a_2)								
20	135.81(a_1)		401						
	136.42(a_2)								
21	139.42		203						
22	141.35(a_1)		222						
	142.34(a_2)								
23	149.16(a_1)		320						
	150.24(a_2)								

[a] The reflections are found in the XRD pattern but were canceled in the data table [1].

form B=B=B double bonds. In the hexagonal model, the distance between B atoms along the *c*-axis is only 0.14 nm, which is small compared with the B–B single bonds in a boron crystal (0.16–0.185 nm) [19]. This agrees with the regularity that, with increasing bond number, the last bond length will decrease. The following analysis will show that the B atoms in the LiB compound are sp^3 hybridization and connected via a bent covalent binding chain B=B=B.

For sp^3 hybridization, the four sp^3 orbits are in tetra-

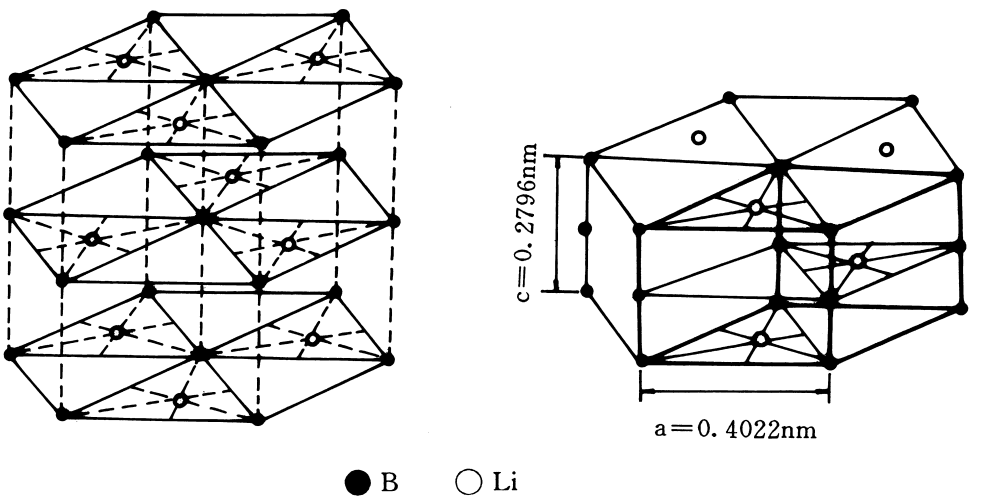

Fig. 5. Unit cell structure model of the LiB compound. B position, (2*b*), (0, 0,1/4); Li position, (2*c*), (1/3,2/3,1/4).

Table 2
Results of the calculation of the XRD intensity[a]

No.	Experimental			Calculation results		
	2θ	I_0	hkl	2θ	I_1	I_2
1	25.47	100	100	25.57	100	100
2	41.30	23.5	101	41.41	20.5	20.5
3	44.98	57.8	110	45.08	61.3	61.3
4	52.44	3.6	200	52.54	4.1	4.1
5	62.77	4.1	201	62.86	4.3	4.3
6	66.87	0.9	002	66.93	0.9	3.7
7	71.59	1.9	120	71.68	2.1	2.1
8	72.84	0.9	102	72.91	0.6	1.8
9	80.59	2.8	121	80.66	3.1	3.1
10	83.09	5.0	300	83.21	5.1	5.1
11	84.22	1.2	112	84.38	6.5	9.2
12	89.95	0.3	202	90.00	0.3	1.0
13	100.05	3.2	220	100.11	2.9	2.9
14	105.82	1	130	105.88	0.7	0.7
15	106.99	0.4	122	107.09	0.4	1.4

[a] Anisotropy temperature parameters: I_1, $\bar{u}_{B\sigma} = 0.009$ nm, $\bar{u}_{Bc} = 0.020$ nm, $\bar{u}_{Li\sigma} = \bar{u}_{Lic} = 0.007$ nm, $R_{B1} = 0.068$; I_2, $\bar{u}_{B\sigma} = \bar{u}_{Bc} = 0.009$ nm, $\bar{u}_{Li\sigma} = \bar{u}_{Lic} = 0.007$ nm, $R_{B2} = 0.109$; $R_B = \Sigma|I_E - I_C|/\Sigma I_E$.

hedral geometry with an angle of 109°26′ between any two orbits. The bent covalent bond [20] is shown in Fig. 6, where the arc length l is the length of a B–B single bond, and distance r is the length of the bent bond. Because the B atom is an electron-deficient element, the B–B bond distance depends on its near neighbor atom number and hybridized state. In the α-tetragonal boron crystal unit cell, there are two boron atoms having four covalent bonds with tetrahedral geometry [19], corresponding to sp^3 hybridization. The corresponded bond length is 0.16 nm. Taking 0.16 nm as the B–B single bond length l, the bent bond length r is easily calculated [20]. The calculated result is 0.138 nm, which is close to the result of 0.14 nm from the hexagonal model.

The crystal structure of the LiB compound shown in Fig. 5 is isomorphic with the graphite structure. The unit cell is small. The B atoms occupy the (2*b*) site (0,0,1/4) and the Li atoms occupy the (2*c*) site (1/3,2/3,1/4). It also belongs to No.194 space group $P6_3/mmc$ [21].

4.3. Neutron diffraction intensity

Neutron diffraction is a very important means to study crystal structure. According to the unit cell model of LiB in this paper, and the experimental conditions in Wang and Mitchell's work [1], $\mu T = 0.57$, $b_{Li} = -0.214$, $b_B = 0.65$ and $\lambda = 0.11422$ nm, the neutron diffraction intensity (I_c) can easily be calculated [1,22].

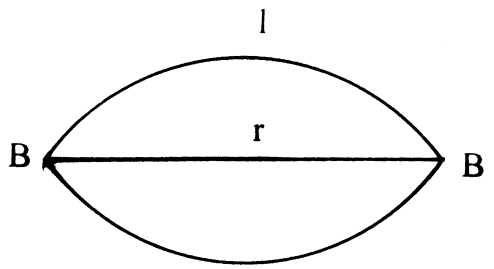

Fig. 6. Bent covalent bond assumption for the boron covalent bond.

The result is shown in Table 3. Wang and Mitchell [1] pointed out that the ''anomalous'' reflections in the XRD spectrum (101, 201 and 121 reflections) disappeared in neutron diffraction. But our computation result shows that those reflections exist. The texture is very easily formed in the Li–B alloy under deformation, which leads to the absence of some reflections, which will be discussed in the next section.

4.4. Density

The theoretical density of the LiB compound can be calculated according to the hexagonal structure model. The actual density of LiB has to be calculated from the experimental density of Li–B alloy. For specimen 2 (Li–33 wt% B), the actual density of LiB is derived from the density (0.83 g/cm^3) of Li–B alloy in which the effect of O and Mg is considered. For the data of Sanchez and Belin [9] (Li–33.5 wt% B), it is derived from the data that, after extracting free lithium with tetrahydrofuran (THF)–naphthalene solution, the remaining frame has porosity 0.671 and apparent density 0.47 g/cm^3. For the data of Mitchell and Sutula [17] (Li–30 at% B), it is derived from the density (0.92 g/cm^3) of extruded Li–B alloy. All the results are summarized in Table 4. Both theoretical and experimental results fit well.

4.5. Morphology and texture of the LiB compound

Although the diffraction indices of LiB satisfy the extinction rule of a close-packed hexagonal system, its

Table 3
Results of neutron diffraction calculation

No.	Calculation			Experimental[a]	
	2θ (°)	I_c (%)	hkl	2θ (°)	I_0 (%)
1	18.87	100	100	18.83	100
2	30.34	4.8	101		
3	33.00	10.7	110	32.93	13
4	38.29	24.6	200	38.20	23
5	45.43	2.2	201		
6	48.15	1.7	002		
7	51.42	27.9	210	51.33	28
8	52.16	27.1	102		
9	57.30	2.9	121		
10	58.93	3.4	300	58.80	15
11	59.61	6.6	112		
12	63.21	19.0	202		
13	69.21	2.5	220	69.06	6
14	72.50	14.9	130	72.33	14
15	73.09	29.5	122		

[a] Anisotropy temperature parameters: $\bar{u}_{B\sigma} = \bar{u}_{Bc} = 0.009$ nm, $\bar{u}_{Li\sigma} = \bar{u}_{Lic} = 0.007$ nm.

Table 4
Density of the LiB compound (g/cm^3)

Ideal model	Sample 2	Sanchez [9]	Mitchell [17]
1.50	1.49	1.43 1.49[a]	1.47

[a] Corrected according to the shrinkage ratio of Li–B alloy in Mitchell and Sutula's work [20].

axial c/a ratio is only 0.70, with close-packed direction ⟨001⟩. According to the general rule, the crystal is easy to grow along the closed packed direction. The crystal of LiB may therefore grow anisotropically to form fibers. In sample preparation, LiB is formed in the second exothermic reaction (~530°C), because the reaction is instantaneous, no method can be used to control its nucleation and growth. The morphology of LiB as shown in Fig. 4 is in its natural state with fibrous structure. Sanchez and Belin [9] reported the fibrous characteristic of LiB. SEM pictures (Fig. 4) clearly show that LiB is in the form of fibers and the fibers align along the rolling direction after rolling (Fig. 4). When $l \neq 0$, all the crystal planes (hkl) are not parallel to the rolling plane, which leads to the absence of corresponding diffraction reflections (Fig. 2). This is also evidence for our theoretical model of the unit cell of LiB.

In the determination of crystal structures, single crystals are very important to make the measurements more direct and easier. Unfortunately, success in producing a LiB single crystal has not been reported. The strong texture of LiB mentioned above is in the middle state between an ideal single crystal and a polycrystal. For LiB, the main anisotropy is in the directions ⟨0001⟩ and ⟨hki0⟩. Therefore, the rolling texture can be treated approximately as a wire texture. Fig. 7 shows a comparison between calculated diffraction point positions for a wire texture and the practical diffraction circle. Both fit well.

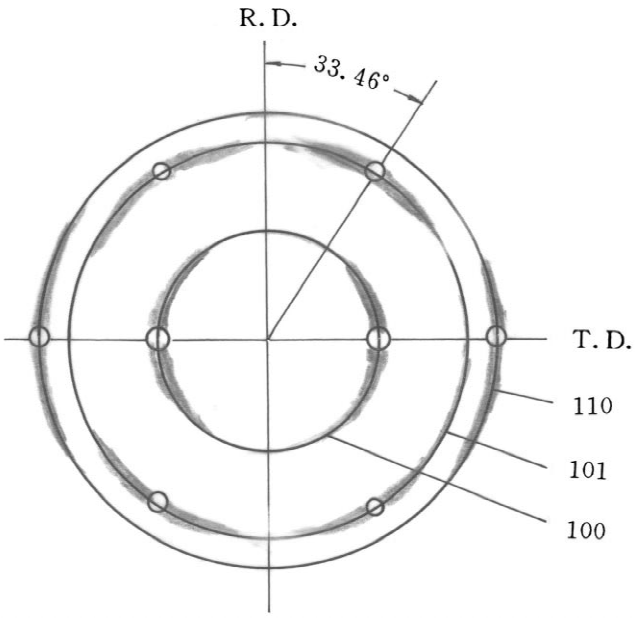

Fig. 7. Comparison between theoretical wire texture diffraction spots and experimental diffraction circles.

5. Conclusions

1. In the Li–B alloys used for anode materials of thermal batteries, the refractory and porous frame consists of the compound LiB. LiB belongs to the hexagonal system, space group (No. 194) $P6_3/mmc$ with lattice constants $a = 0.4022$ nm and $c = 0.2796$ nm. In the unit cell, B atoms occupy the (2b) site (0,0,1/4) and Li atoms occupy the (2c) site (1/3,2/3,1/4); the theoretical density is 1.50 g/cm^3.
2. Boron atoms in the compound are covalently bonded to each other in the ⟨001⟩ direction with B=B=B chains and lithium is Li^+.
3. The morphology of the compound is fibrous. After rolling, the fibers align along the rolling direction. XRD patterns and the Laue photograph show the corresponding texture phenomenon, which fits well with the theoretical prediction.

References

[1] F.E. Wang, M.A. Mitchell, R.A. Sutula, J.R. Holden, J. Less Common Met. 61 (1978) 237–251.
[2] S. Dalleck, D.W. Ernst, B.F. Larrick, J. Electrochem. Soc. Solid-state Sci. Technol. 126 (5) (1979) 866.
[3] T. Marcac, P. Bukovec, N. Bukovec, Thermochim. Acta 133 (1988) 305.
[4] V.P. Sorokin, P.J. Gavriolv, E.V. Levakov, Russ. J. Inorg. Chem. 22 (1977) 329, English translation.
[5] F.E. Wang, US Patent 4,110,111 (1978).
[6] C.S. Winchester, in: Proceedings of the 30th Power Sources Conference, 1982, p. 23.
[7] F.E. Wang, Metall. Trans. A 10A (1979) 343.
[8] S.D. James, L.E. Devries, J. Electrochem. Soc. 123 (1976) 321.
[9] P. Sanchez, C. Belin, G. Crepy, A. De Guibert, J. Mater. Sci. 27 (1992) 240.
[10] W.P. Kilroy, I. Angres, J. Less Common Met. 63 (1979) 123.
[11] Powder Diffraction File, International Center for Diffraction Data, PA, USA, 1995, 15-401.
[12] Powder Diffraction File, International Center for Diffraction Data, PA, USA, 1995, 12-254.
[13] G. Mair, R. Nesper, H.G. Von Schnering, J. Solid State Chem. 75 (1988) 30.
[14] H.P. Klug, L.E. Alexander, X-ray Diffraction Procedures, 2nd Edition, Wiley, New York, 1974.
[15] C. Kittel, Introduction To Solid State Physics, 5th Edition, Wiley, New York, 1976.
[16] R. Telle, in: M.V. Swaim (Ed.), Structure and Properties of Ceramics, Materials Science and Technology, Vol. 11, VCH, New York, 1994, p. 186.
[17] M.A. Mitchell, R.A. Sutula, J. Less Common Met. 57 (1978) 161.
[18] U. Muller, Inorganic Structural Chemistry, Wiley, Chichester, 1993.

[19] Y. Gong, Boron, Inorganic Chemistry Series, Vol. 2, Science Press, Beijing, 1987, in Chinese.
[20] P. Yang, X. Gao, Chemical Bonding and Structure Property Relations, Advanced Education Press, Beijing, 1987, in Chinese.
[21] T. Hahn (Ed.), Space Group Symmetry, International Tables for Crystallography, Vol. A, D. Reidel, Dordrecht, 1993, p. 590.
[22] C.G. Bacon, Neutron Diffraction, 3rd Edition, Clarendon Press, Oxford, 1975.